



**Algorithm Document
TOSOMI**

REF : TEM/AD3/002
ISSUE : 1.0
DATE : 09.08.06
PAGE : 1/28

TITLE:

Algorithm Document

TOSOMI

Authors :

H.J. Eskes (KNMI)
R.J. van der A (KNMI)
E. Brinksma (KNMI)

	Algorithm Document TOSOMI	REF : TEM/AD3/002 ISSUE : 1.0 DATE : 09.08.06 PAGE : 2/28
---	--	--

DOCUMENT STATUS SHEET

Issue	Date	Modified Items / Reason for Change
0.9	20.01.06	First Version
1.0	09.08.06	Corrections based in response to the review of J.-C. Lambert

TABLE OF CONTENTS

1.1	Forward model and inversion procedure	3
1.1.1	<i>Introduction</i>	3
1.1.2	<i>Description of method and implementation</i>	3
1.1.3	<i>TOSOMI</i>	15
1.2	Auxiliary data	16
1.2.1	<i>Specification of the GTOPO30 climatology</i>	16
1.2.2	<i>Specification of combined GOME/TOMS albedo climatology</i>	17
1.3	Sensitivity and Error analysis	17
1.4	Validation with groundbased observations	18
1.4.1	<i>Approach</i>	18
1.4.2	<i>Validation results</i>	18
1.5	Recommendations for product validation	25
1.6	References	25

	Algorithm Document TOSOMI	REF : TEM/AD3/002 ISSUE : 1.0 DATE : 09.08.06 PAGE : 3/28
---	--	--

1.1 Forward model and inversion procedure

1.1.1 Introduction

The Sciamachy total ozone retrieval algorithm TOSOMI (Total Ozone retrieval scheme for SCIAMACHY based on the OMI DOAS algorithm) is an application of the TOGOMI algorithm to SCIAMACHY.

The new GOME algorithm TOGOMI [Valks and Van Oss, 2003] is based on the total ozone DOAS (Differential Optical Absorption Spectroscopy) algorithm developed for the OMI instrument [Veefkind and De Haan, 2001]. With respect to total ozone column retrieval using the DOAS method, the OMI, SCIAMACHY and GOME instruments are very similar. The main improvements of the new algorithm are:

- (i) treatment of the atmospheric temperature sensitivity by using effective ozone cross-sections calculated from ECMWF temperature profiles,
- (ii) improvements in the calculation of the air mass factor, using the so-called empirical approach,
- (iii) using the Fast Retrieval Scheme for Clouds from the Oxygen A-band (FRESCO) algorithm for the cloud correction,
- (iv) a new treatment of Raman scattering in DOAS [De Haan, 2003]. This new formulation of DOAS explicitly accounts for the smearing of the solar Fraunhofer lines as well as the atmospheric tracer absorption structures, and
- (v) air-mass factors based on semi-spherical polarization-dependent radiative transfer (KNMI DAK model).

The SCIAMACHY total ozone retrieval algorithm TOSOMI combines a Sciamachy level-1 product reading module with the TOGOMI DOAS modules. The Fresco algorithm [Koelemeijer, 2001] is applied to the Sciamachy spectra to obtain cloud fraction and cloud top height estimates.

1.1.2 Description of method and implementation

The TOGOMI total ozone algorithm consists of four steps. First, the GomeCal package is applied to the GDP-level-1 files to improve the accuracy of the measured Earth radiance and solar irradiance spectrum. In the second step, the DOAS method is used to fit the reference differential absorption spectrum of ozone to the measured Earth radiance spectrum and solar irradiance spectrum, to obtain the slant column density. In the third step the slant column density is translated into the vertical column density using the so-called air mass factor (AMF). The fourth step consists of a correction for cloud effects. In this section we describe each of these retrieval steps, including the physical background, as well as assumptions and *a priori* information used.

	Algorithm Document TOSOMI	REF : TEM/AD3/002 ISSUE : 1.0 DATE : 09.08.06 PAGE : 4/28
---	--	--

1.1.2.1 Improvement of GOME level-1 spectra

The input for the new TOGOMI algorithm is based on the GOME level-1 product as produced by the GDP, but with several improvements. To improve the wavelength calibration of the Earth radiance and solar irradiance spectra, the GomeCal package is applied to the GDP level-1 files [Van Geffen, 2003a]. In addition to a wavelength re-calibration, GomeCal applies an improved polarisation correction to the GDP level-1 spectra and a radiometric correction, which includes a correction for the degradation of the GOME instrument.

The standard wavelength calibration of the GDP uses spectral lines of an onboard PrCr/Ne hollow cathode lamp to correct for shifts in the wavelengths associated with the detector pixels, for example caused by temperature effects, with respect to a pre-flight calibration. This calibration is not accurate enough for the retrieval of the DOAS total ozone product. A new calibration method, developed by Van Geffen [2003b], uses as reference spectrum a high-resolution solar spectrum, with irradiance values given at 0.01 nm intervals.

To be able to fit the observations with this reference spectrum, i.e. with the Fraunhofer lines in the solar spectrum, the reference spectrum is convolved with the GOME slit function and subsequently integrated over the spectral bins of the detector. The location and width of these bins are allowed to vary along the detector: both a shift and a squeeze are applied to the measurements (the GDP calibration method with the lamp lines applies only a shift), where the GDP's wavelength grid serves as the initial guess. The improved wavelength grid is found with a tailor-made chi-square minimisation. The method provides a calibration accuracy of 0.001 nm or better above 290 nm, corresponding to about 1/100th of a pixel for the DOAS fitting window. The calibration can be applied to a user specified wavelength window, thus optimising the calibration for subsequent retrieval purposes.

When extracting the GDP level-1 spectra, a polarisation correction can be applied, based on a theoretical value at 300 nm (UV) and polarisation measurements in 100 nm wide windows around 350, 500 and 700 nm. This correction, however, appears to be insufficient, in particular in the UV range. Schutgens and Stammes [2002] developed an improved polarisation correction which replaces the GDP's correction. The new polarisation correction is based on a parametrisation of the UV Earthshine polarisation between 290 and 330 nm, as function of solar zenith angle, viewing geometry, scene albedo and total ozone column. For wavelengths above 330 nm the method supplies the same polarisation correction as the GDP.

The calibration of the absolute (ir)radiance in the GDP level-1 spectra appears to be insufficiently accurate. Additionally, it has been observed that the GOME instrument shows a degradation, notably since 1998. This degradation is time and wavelength dependent, and the measured earthshine radiances degrade differently from the solar irradiance spectra. The degradation is only partly corrected for when extracting GDP level-1 spectra. In the GOME instrument, Peltier elements are used for cooling the detector. There is some interference of the Peltier cooler conduct signals on the detector signals, for which a correction is included in the standard calibration of the GDP, but this correction does not remove all interference effects.

For these reasons, a radiometric correction procedure was made by Van der A [2001] consisting of three parts which can be applied independently, in addition to the corrections of the GDP extractor:

- a radiometric calibration

	Algorithm Document TOSOMI	REF : TEM/AD3/002 ISSUE : 1.0 DATE : 09.08.06 PAGE : 5/28
---	--	--

- a correction for the degradation of the instrument
- a correction to remove residual effects of the interference of the Peltier cooler signals

The first two corrections apply to wavelengths between 265 and 390 nm and correction data are available up to 1 July 2001; for dates after that, the correction of 1 July 2001 is used (the lack of good measured solar spectra severely hinders determining correction data after 1 July 2001).

1.1.2.2 Slant Column Density

The first step in the ozone DOAS algorithm is to determine the slant column density. The slant column density is the amount of ozone along an average path that the photons travel from the Sun, through the atmosphere, to the satellite sensor. The slant column density is determined by fitting an analytical function to the measured Earth radiance and solar irradiance data. This fit is applied to data taken in a certain wavelength range, called the fit window. A polynomial function, which serves as a high-pass filter, is applied to account for scattering and absorption that vary gradually with the wavelength, e.g., scattering by molecules, aerosols, and clouds. The slant column density is derived from the filtered data, which contains spectral features of ozone in the fit window. Figure 1 shows a DOAS fit applied to GOME level-1 data.

1.1.2.2.1 Basic concept

A nadir-viewing instrument like GOME measures the radiance reflected by the Earth and the atmosphere. For spectral ranges where ozone causes the dominant spectral absorption features, the top-of-the-atmosphere reflectance (TOAR) can be approximated by:

$$\rho(\lambda, \theta_0, \theta, \varphi - \varphi_0) = \frac{\pi I}{F_0} = P(\lambda) e^{-\sigma_{O_3}(\lambda) N_s} \quad [3-1]$$

where ρ is the top-of-the-atmosphere reflectance, I is the Earth radiance, λ is the wavelength, θ_0 is the solar zenith angle; θ is the viewing zenith angle; $\varphi - \varphi_0$ is the relative Sun-satellite azimuth angle; $F_0(\lambda)$ is the extraterrestrial solar irradiance per unit area of the atmosphere, $\sigma_{O_3}(\lambda)$ is the ozone absorption cross section, N_s the ozone slant column density and $P(\lambda)$ is a low order polynomial that acts as high-pass filter. Equation [3-1] holds for optically thin absorbers and is inspired by the well-known Lambert-Beer law and photon path distributions [Van de Hulst, 1980]. Numerical experiments using radiative transfer calculations (excluding Raman scattering, see next Section) have shown that for ozone absorption in the Earth atmosphere, equation [3-1] is an accurate approximation for wavelengths longer than approximately 320 nm.

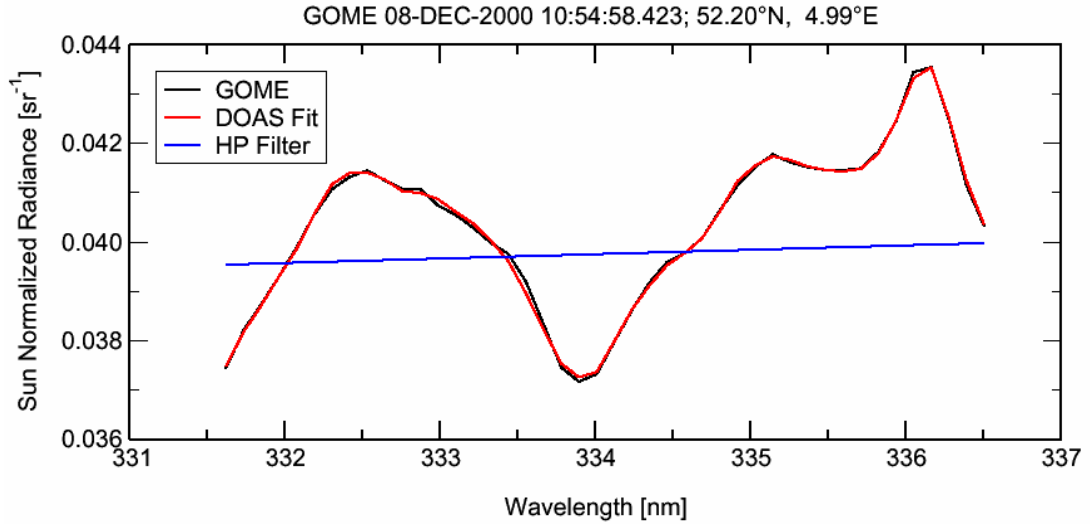


Figure 1 DOAS fit applied to GOME data measured over western Europe on December 8, 2000. The spectral resolution of the GOME data was decreased by a low pass filter to avoid undersampling. The black line shows the Sun normalized radiance measured by GOME, the red line shows the DOAS fit of the measured data. The blue line shows the high-pass filter that was used in the fit.

1.1.2.2.2 Ring effect: Raman scattering

One of the assumptions underlying Equation [3-1] is that scattering on air molecules is elastic. This is, however, not completely true. About 4% of all scattering events on air molecules are inelastic, resulting in a shift in the photon wavelength upto 2 nm. The most pronounced consequence on the diffuse radiation field is that the solar Fraunhofer lines are smeared-out. However, the atmospheric absorption structures are influenced as well, resulting in more-shallow line depths. This has an immediate effect on DOAS trace gas retrievals in case Raman scattering is not taken into account, leading to too-small columns. This error amounts to several percent, motivating a proper treatment of this effect.

We follow the approach introduced by *de Haan* [2003] to deal with Raman scattering in the ozone column retrieval. Equation [3-1] is adjusted to account for Raman scattering by adding a term corresponding to inelastic scattered radiation:

$$\frac{I_{\text{det}}^{\text{meas}}(\lambda)}{F_0^{\text{meas}}(\lambda)} = P_{\text{el}}(\lambda) \left(\exp[-N_s \sigma_x^{\text{el}}(\lambda)] + \frac{P_{\text{inel}}(\lambda)}{P_{\text{el}}(\lambda)} \frac{I_{\text{Ring}}^{\text{eff}}(\lambda)}{F_0^{\text{meas}}(\lambda)} \exp[-N_s \Delta\sigma_x^{\text{eff}}(\lambda)] \right) \quad [3-2]$$

Here, $P_{\text{el}}(\lambda)$ and $P_{\text{inel}}(\lambda)$ are low degree polynomials of the wavelength, representing the overall wavelength dependence due to scattering, $\sigma_x^{\text{el}}(\lambda)$ is the effective absorption cross section of the trace gas for elastic scattering, $I_{\text{Ring}}^{\text{eff}}(\lambda)$ is the commonly used Ring spectrum due to Fraunhofer lines in the solar irradiance. Furthermore,

	Algorithm Document TOSOMI	REF : TEM/AD3/002 ISSUE : 1.0 DATE : 09.08.06 PAGE : 7/28
---	--	--

$$\Delta\sigma_x^{eff}(\lambda) = (\mu_0 \sigma_x^{ns}(\lambda) + \mu \sigma_x^s(\lambda)) / (\mu + \mu_0), \quad [3-3]$$

with $\sigma_x^s(\lambda)$ and $\sigma_x^{ns}(\lambda)$ effective cross sections involving high-resolution solar spectrum and the Raman spectrum, see *de Haan* [2003] for further details; μ_0 is the cosine of the solar zenith angle and μ is the cosine of the viewing angle. Equation [3-2] has been derived starting with two simplifications: (1) the absorber is situated complete above the scattering layer, and (ii), observed radiation is scattered only once (elastic or inelastic). In this situation an algebraic solution for the radiance can be found. Both simplifications are then subsequently left and the resulting implications for the solution are carefully evaluated.

1.1.2.2.3 Instrumental Errors

The TOGOMI algorithm uses corrected GDP level 1-data of the backscattered Earth radiance and the solar irradiance as input. These data contains random and systematic errors. However, DOAS is not affected by systematic errors unless they produce structures that are correlated with ozone absorption spectrum.

For GOME, most of the optical path is the same for the Earth radiance and solar irradiance measurements. Dividing the measured Earth radiance by the measured solar irradiance will lead to a cancellation of errors due to components that are in the optical paths of both the radiance and irradiance measurement. The radiometric accuracy of the TOAR is therefore higher than for the separate radiance or irradiance measurement [*Levelt et. al*, 2000].

The DOAS method is insensitive to radiometric calibration errors that are multiplicative and constant with wavelength. However, the method is sensitive to additive radiometric errors (offsets). Offsets in the Earth radiance can be accounted for by adding a fit parameter c_a ¹:

$$\rho(\lambda, \theta_0, \theta, \varphi - \varphi_0) = \{RHS Eq.[2.2]\} + c_a / F_0(\lambda). \quad [3-4]$$

Note that in the last term of equation [3-4] $F_0(\lambda)$ is the solar irradiance measured by GOME.

If the GOME radiance or irradiance data show radiometric errors with spectral structure in the DOAS fit window, it depends on the spectral features whether a correction can be made. If the spectral feature is weak, well characterized and doesn't interfere with the ozone absorption cross section, it may be possible to account for it in the fit. In this case, the spectral structure of the error is fitted in the DOAS equation using an extra fitting parameter. Errors that interfere with the ozone absorption cross section cannot be corrected for. If this happens, another fit window should be used that does not show such an interference.

1.1.2.2.4 Ozone absorption cross-section and temperature dependence

The accuracy of the slant column retrieval depends on the accuracy and suitability of the laboratory absorption cross-section data used in the DOAS fit. Ozone absorption cross-sections have been measured as

¹ The behavior of the fit parameter c_a over the lifetime of GOME may be used to monitor the long term stability of the instrument. It is not possible to add a fit parameter to account for offsets in the measured solar irradiance, because this results in an unstable fit. However, the solar irradiance is well known and the expected offset in the solar irradiance measurements is small

	Algorithm Document TOSOMI	REF : TEM/AD3/002 ISSUE : 1.0 DATE : 09.08.06 PAGE : 8/28
---	--	--

a function of wavelength and temperature. For the TOGOMI algorithm, two well-established data sets of ozone absorption cross-sections are considered: the GOME Flight Model (FM98) and Bass and Paur (B&P) cross-sections. The FM98 cross-sections have been measured at 5 different temperatures during the pre-flight calibration using the GOME flight model [Burrows *et al.*, 1999b]. The B&P cross-sections [Bass and Paur, 1986] have been measured at high resolution (better than 0.025nm) and have been recently recommended as a standard for use in remote-sensing applications [Orphal, 2002].

The study of the accuracy of GDP v3 total ozone product by Van Roozendael *et al.*, [2002] shows the importance of the cross-section quality and the treatment of the temperature dependence in the DOAS fit. This study indicates that the use of FM98 cross-sections results in a high quality and stable DOAS fit when applying a fixed shift of +0.017 nm to the cross-sections. To account for the temperature dependence, an effective ozone absorption cross-section is calculated using daily temperature analyses (or forecast) from the European Centre for Medium-Range Weather Forecasts (ECMWF) model:

$$\sigma_{o_3,eff}(\lambda) = \frac{\int \rho(z) \sigma_{o_3}(T(z), \lambda) dz}{\int \rho(z) dz} \quad [3-5]$$

where $\rho(z)$ is the ozone concentration at altitude z , here determined from an ozone profile climatology from Fortuin and Kelder [1998], and $\int \rho(z) dz$ is the corresponding vertical ozone column. $T(z)$ is the ECMWF temperature at altitude z (the new ECMWF model provides temperatures for 60 vertical levels), and $\sigma_{o_3}(T(z), \lambda)$ is the temperature dependent ozone absorption cross-section. The resulting effective cross-section $\sigma_{o_3,eff}$ is used in equation [3-4] to calculate the ozone slant column density.

To avoid problems due to the uncertainty in the GOME slit function and the GOME undersampling, the effective spectral resolution of the GOME spectra and the cross-sections is reduced by applying a low pass filter. An advantage of this procedure is that the effective slit function is known very accurately, as it is determined by the low pass filtering. For ozone retrieval in the Huggins band, an effective slit function with a FWHM up to 0.6 nm can be used [Burrows *et al.*, 2002].

1.1.2.2.5 Fit window

In this section we describe the fit window choice for the TOGOMI algorithm. Detailed studies were performed to select suitable fit windows for ozone with respect to the following [Veefkind, 2000a,b,c]:

- Temperature profile
- Instrument signal-to-noise
- Ozone profile
- Other trace gases
- Ring effect.

The conclusions of these studies are that the main drivers for the fit window choice are the sensitivity of the slant column density to atmospheric temperature and to instrument signal-to-noise. The temperature sensitivity is small for narrow fit windows in distinct wavelength regions. On the other hand, the effect of signal-to-noise is less for wider fit windows. The current GOME ozone fitting window, as used in the GDP v3, is 10 nm wide, centered around 330 nm. This is a temperature sensitive fit window with a high

	Algorithm Document TOSOMI	REF : TEM/AD3/002 ISSUE : 1.0 DATE : 09.08.06 PAGE : 9/28
---	--	--

s/n ratio. In the TOGOMI algorithm, the temperature sensitivity is taken into account by using an effective ozone cross-section, as described in the previous section.

A good compromise between temperature dependence and signal-to-noise was found to be a 5 nm wide window centered around 334.1 nm. Although the differential absorption of ozone is smaller compared to the current GOME window, the effects of the instrument signal-to-noise on the slant column density are still below 1% [Veeffkind, 2000b]. Both the wide and narrow fit windows are implemented in the TOGOMI algorithm.

1.1.2.2.6 Fit Method

The slant column density is determined by fitting equation [3-4] to the measured TOAR for the fit window. As described in Section 3.2.2.4, first the effective spectral resolution of the TOAR and the cross-sections is reduced by applying a low pass filter. Then, the fit is performed using a least squares fitting procedure, which minimizes the merit function given by:

$$\chi^2 = \sum_{i=1}^N \left(\frac{y_{meas}(\lambda_i) - y_{sim}(\lambda_i)}{\epsilon_{meas}(\lambda_i)} \right)^2, \quad [3-6]$$

where, $y_{meas}(\lambda_i)$ is the measured TOAR, $y_{sim}(\lambda_i)$ is the simulated TOAR radiance as given by Eq. [3-4] and $\epsilon_{meas}(\lambda_i)$ is the precision of the measured TOAR. The fit window is between λ_1 and λ_N .

The simulated TOAR (Eq. [3-4]) is a non-linear function of the fit parameters. Therefore, a non-linear fit routine should be applied. A modified Levenberg-Marquardt method [More, 1978], as adapted from the SLATEC mathematical library [Fong *et al.*, 1993], is used for the non-linear fitting. Information on the quality of the fit is derived from the covariance matrix. The variance of the fitted parameters, as well as the correlation between them, is also obtained from the covariance matrix.

1.1.2.3 Air Mass Factor (AMF)

In the ozone DOAS algorithm, the air mass factor is used to translate the slant column density into a vertical column density. The air mass factor M is defined as the ratio of the slant column density, N_s , and the vertical column density, N_v , i.e.,

$$M \equiv \frac{N_s}{N_v} \quad [3-7]$$

The DOAS fit results in one slant column density for the entire fit window. From the definition of the AMF (Eq. [3-7]) it is clear that there is also one AMF for a fit window.

The AMF depends on the Sun-satellite geometry, as well on the “state of the atmosphere”. With the latter it is meant that AMF depends on the ozone profile, on clouds and aerosol properties, on surface reflectivity properties etc.. Often, the AMF will vary approximately as the geometrical AMF, $M_g = \sec(\theta) + \sec(\theta_0)$. To eliminate most of the geometrical effects, it is convenient to introduce an effective AMF, M_e , defined as

	Algorithm Document TOSOMI	REF : TEM/AD3/002 ISSUE : 1.0 DATE : 09.08.06 PAGE : 10/28
---	--	---

$$M_e = \frac{M}{M_g}$$

[3-8]

1.1.2.3.1 Computation

The AMF can be determined using a radiative transfer model and a GOME simulator. The radiative transfer model produces radiances for a model atmosphere. The GOME simulator is used to produce spectra with the resolution and sampling of GOME. We determine the slant column density by fitting DOAS to these spectra and divide by the known vertical column density to determine the airmass factor. The advantage of this procedure is that exactly the same DOAS fit is applied to the synthetic GOME spectra and to the measured GOME spectra. If the model atmosphere is representative of the 'real' atmosphere, this may lead to a cancellation of certain errors.

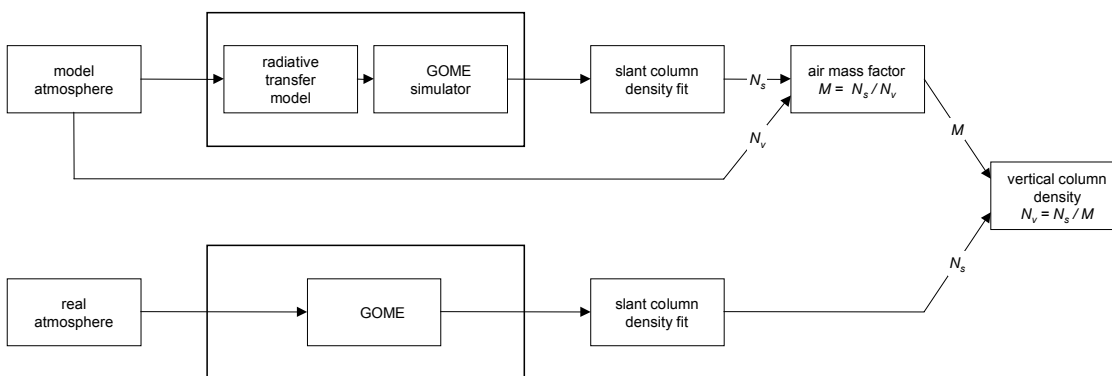


Figure 2 Schematic of the empirical DOAS method for GOME.

The AMF depends, among other parameters, on the ozone profile. The ozone profiles in the atmosphere vary strongly, resulting in changes of several percent in the effective air mass factor, depending on the Sun-satellite geometry. To reduce the uncertainty in the AMF due to the ozone profile, a slant column density dependent AMF is used. To derive a relation between the slant column density and the AMF, a set of ozone profiles is used that cover the natural variability of the ozone profile for a given location and time period. For each of these profiles the AMF is calculated for a given Sun/satellite geometry and surface properties. This procedure is illustrated in Figure 3. The top panel shows a set of ozone profiles that are representative for 55°N for December. These profiles are taken from the ozone profile climatology from Logan, Labow & McPeters as used in the TOMS V8 total ozone algorithm. This climatology contains 3 (at low-latitudes) to 10 (at high-latitudes) column classified ozone profiles per 10° latitude band for each month. The bottom panel of Figure 3 shows the effective AMF for each of the profiles, plotted as a function of slant column density. As can be seen in Figure 3, the effective AMF varies almost linearly with the slant column density. This is used in the TOGOMI algorithm, by making the effective AMF a linear function of the slant column density determined in the DOAS fit, as indicated in the bottom panel. This method thus reduces the uncertainty in the AMF due to ozone profile changes with respect to the climatology. The algorithm uses a look-up-table (LUT) of effective AMFs. By using a look-up-table, no radiative transfer calculations have to be done on-line, which results in better performance.

	Algorithm Document TOSOMI	REF : TEM/AD3/002 ISSUE : 1.0 DATE : 09.08.06 PAGE : 11/28
---	--	---

1.1.2.3.2 Radiative transfer model

The radiative transfer model used for the simulations of spectra and, consequently, for the calculation of the AMFs (see Fig.2) is the Doubling-Adding-KNMI (DAK) model [De Haan *et al.*, 1987; Stammes *et al.*, 1989; and Stammes *et al.*, 2001]. Single scattering properties of aerosol particles and PSCs are calculated with a Mie scattering code [De Rooij and Van der Stap, 1984] that generates coefficients for the expansion in generalized spherical functions. These functions can directly be read by the DAK code making efficient calculations for polarized light possible. Note that the T-matrix code for non-spherical particles of Mishchenko produces similar output in terms of generalized spherical functions, which makes calculations for non-spherical particles straightforward (see e.g. Mishchenko and Travis [1998]). The code has the advantage that it is fast for cloudy atmospheres, is well suited for polarized radiative transfer calculations and is very accurate for relatively simple atmospheric models such as homogeneous cloud layers. Recently, the DAK model has been extended so that a (quasi) spherical geometry can be used. Note that a change in code will only affect the look up tables and does not change the algorithm itself, which means that the code can be replaced at a relatively late moment.

1.1.2.3.3 Look-up-Table

The look-up-table contains the effective AMFs as function of Sun-satellite geometry, surface reflectivity, surface pressures and ozone profile. As mentioned above, the ozone profiles are taken from the Logan, Labow & McPeters climatology. Besides ozone, molecular scattering and absorption by NO₂ and BrO are accounted for in the radiative transfer calculations. Clouds are represented by Lambertian surfaces with an albedo 0.8, as recommended by Koelemeijer and Stammes [1999].

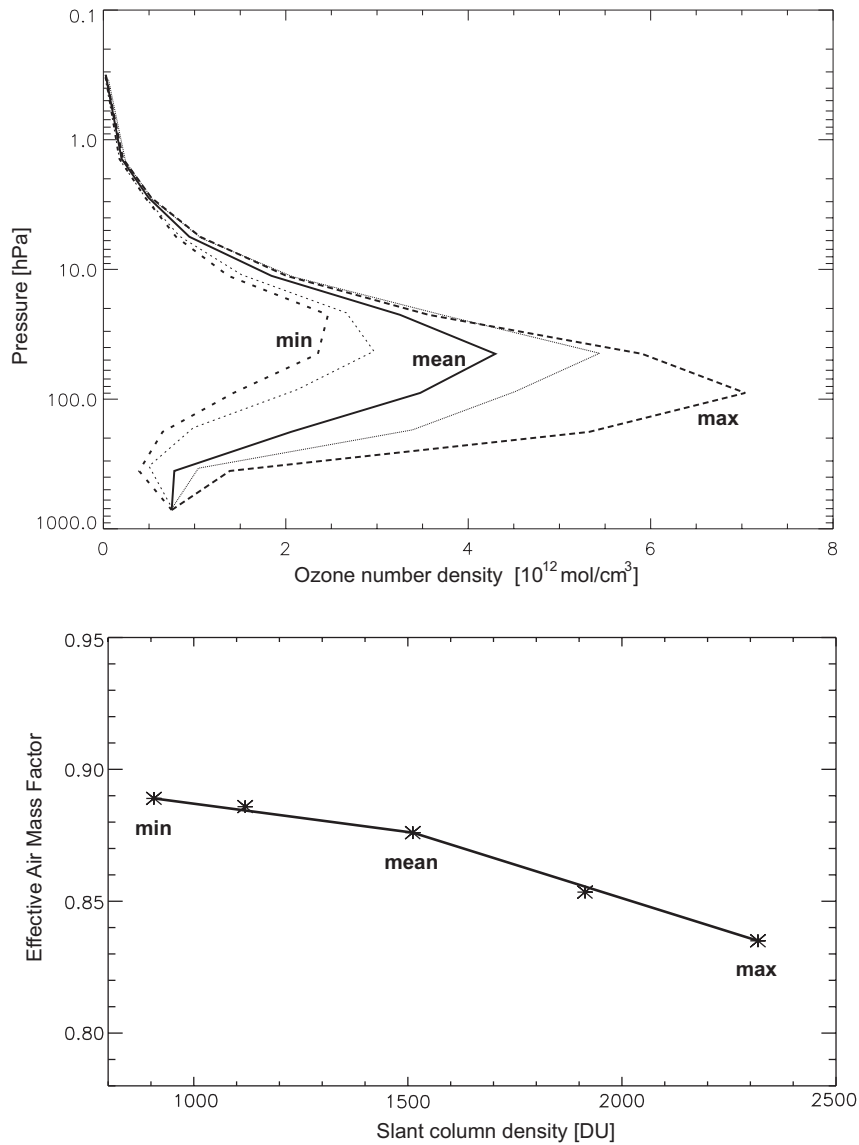


Figure 3. Top panel: Five ozone profiles from the Logan, Labow & McPeters climatology [see Bhartia and Wellemeyer, 2002] for 55°N for December. The thick lines denote the ozone profiles with the smallest vertical columns density ($N_v=225$ DU), an average ozone profile ($N_v=375$ DU), and the ozone profile with the largest vertical columns density ($N_v=575$ DU). Two additional ozone profiles with $N_v=275$ DU and $N_v=475$ DU are also plotted. Bottom panel: Effective AMF computed for the five ozone profiles shown in the top panel, plotted as a function of the slant column density. The effective AMFs have been calculated for a solar zenith angle of 75° and a surface albedo of 0.05, using the 325-335 nm DOAS fit-window.

	Algorithm Document TOSOMI	REF : TEM/AD3/002 ISSUE : 1.0 DATE : 09.08.06 PAGE : 13/28
---	--	---

Table 1.1. *Specification of the air mass factor look-up-table dimensions.*

Dimension name	Min. value	Max. value	Number of entries
Solar zenith angle	0°	89.25°	11
Viewing zenith angle	0°	89.25°	11
Relative azimuth angle	0°	180°	7
Surface reflectivity	0	1.0	5
Surface pressure	126 hPa	1013 hPa	4
Latitude	-90°	+90°	18
Month	1	12	12
Ozone profile	na	na	3

The AMF is obtained by interpolation in the look-up table. In Table 1.1 the dimensions of the look-up table are presented, as well as the foreseen number of entries for each dimension. The inputs that are needed for the interpolation in this look-up table are taken from the following sources. The solar and viewing zenith angles are taken from the GOME level-1 data. The surface reflectivity is determined from a monthly climatology determined by GOME [Koelemeijer *et al.*, 2003]. The surface pressure will be determined from the terrain height, as contained in the level-1 data. The AMF look-up tables will also be interpolated to the latitude and the date of the measurement. Interpolation between the mean and perturbed ozone profiles is done using the method outlined above, using the slant column density as input.

1.1.2.4 Cloud Correction

In case of a cloudy or partly cloudy pixel, part of the ozone column is covered by clouds. Therefore, a cloud correction is needed, which is described in this section. First we describe the FRESCO cloud algorithm, then the computation of the AMF for a partly cloudy pixel, followed by a description of the correction for the so-called ghost column. Finally, we discuss the computation of the total vertical column density.

1.1.2.5 FRESCO cloud algorithm

To determine the AMF for cloudy conditions, the cloud fraction and cloud pressure are needed, which are derived with the Fast Retrieval Scheme for Clouds from the Oxygen A-band (FRESCO) method [Koelemeijer *et al.*, 2001, 2002]. The retrieval is based on a non-linear least squares fitting of the reflectivity spectrum measured by GOME to a simulated spectrum in the range 758-766 nm, and solving for cloud fraction and cloud top pressure. The cloud model represents clouds by Lambertian surfaces or with a BRDF based on Doubling-Adding and Mie calculations. The cloud fraction is derived assuming a cloud albedo of 0.8, corresponding to an optically thick cloud, and this should therefore be regarded as an effective cloud fraction. This cloud albedo choice has been optimised for ozone air mass factor calculations in the UV, when a ghost-column is added to the derived vertical column density to correct for ozone below the cloud, as described below. In the FRESCO method, it is assumed that the absorption below the cloud may be neglected, which can be justified for optically thick clouds. Choosing a high cloud albedo of 0.8

	Algorithm Document TOSOMI	REF : TEM/AD3/002 ISSUE : 1.0 DATE : 09.08.06 PAGE : 14/28
---	--	---

ensures that the model assumptions are internally consistent. The cloud top pressure is derived from the depth of the oxygen A-band, which depends on the absorption optical thickness above the cloud.

This FRESCO cloud model considers all clouds to be thick, single layer clouds. Partly cloudy pixels are treated as the weighted sum of a clear and a cloudy pixel. Pixels that are fully covered with thin clouds are represented by partly cloudy pixels with a thick cloud. Using this cloud model, the AMFs for fully cloudy conditions are determined using the method described in section 3.2.3. The offline calculated AMFs are stored in a look-up-table. This look-up-table has the same dimensions as listed in Table 1.1, with the difference that the surface pressure is replaced by the cloud pressure and there is a single value of 0.8 used for the albedo of the clouds.

1.1.2.6 Air Mass Factor for Partly Cloudy Conditions

Partly cloudy pixels are treated as the weighted sum of a clear and a cloudy pixel. In good approximation, the AMF of a partly cloudy pixel is the area and radiance weighted sum of the AMF of a clear and a cloudy pixel:

$$M = w \cdot M_{cloudy} + (1 - w) M_{clear}, \quad [3-9]$$

where w is the weighting factor, M_{cloudy} is the AMF for a cloudy pixel and M_{clear} is the AMF for a clear pixel. The AMFs for clear and cloudy conditions are taken from the look-up-tables described above. The weighting factor w in Eq. [3-9] is the fraction of the photons that originates from the cloudy part of the pixel [Martin *et al.*, 2002] and can be expressed as:

$$w = \frac{f_c \langle I_{cloudy}(p_c) \rangle}{\langle I \rangle}, \quad [3-10]$$

where f_c is the cloud fraction, $\langle I_{cloudy}(p_c) \rangle$ is the average radiance over the fit window for a pixel that is fully covered with a cloud that is located at pressure p_c , and $\langle I \rangle$ is the average measured radiance for the pixel. The cloud weighting factor w is calculated offline as function of Sun/satellite geometry, surface albedo and pressure, and cloud fraction and pressure, and stored in a look-up-table.

1.1.2.7 Ghost Column

The cloud model treats a cloud as an opaque Lambertian surface of albedo 0.8. The amount of ozone below this surface is called the “ghost column”. It is computed by integrating the ozone profile from the surface to the cloud pressure. The profiles are taken from the *Fortuin and Kelder* [1998] climatology. Using the standard deviations provided in this climatology, the ghost column is made a function of the slant column density, in a similar way as the AMF is a function of the slant column density. As is the case for the AMF, the ghost column will also be determined by interpolation to the latitude and date of the measurement.

1.1.2.8 Total Vertical Column Density

For the computation of the total vertical column density, three cases can be distinguished:

- cloud-free pixels
- cloud covered pixel

	Algorithm Document TOSOMI	REF : TEM/AD3/002 ISSUE : 1.0 DATE : 09.08.06 PAGE : 15/28
---	--	---

- partly cloudy pixels.

For a cloud free pixel the total vertical column density N_t is given by :

$$N_t = \frac{N_s}{M_{clear}}, \quad [3-11]$$

where N_s is the slant column density and M_{clear} is the AMF for clear atmosphere.

For a cloudy pixel the total vertical column density is given by:

$$N_t = \frac{N_s}{M_{cloudy}} + N_g, \quad [3-12]$$

where N_g is ghost column density. For a partly cloudy pixel the total vertical column density is given by:

$$N_t = \frac{N_s + w \cdot M_{cloudy} \cdot N_g}{M}, \quad [3-13]$$

where the AMF, M , is determined according to equation [3-9]. For a cloud-free scene, Eq. [3-13] reduces to Eq. [3-11], and for fully cloudy pixels it reduces to Eq. [3-12].

1.1.3 TOSOMI

The described TOGOMI algorithm has been used as the basis of the TOSOMI algorithm. The differences between the two algorithms are only on the programming level (e.g. different level 1 reading routines).

	Algorithm Document TOSOMI	REF : TEM/AD3/002 ISSUE : 1.0 DATE : 09.08.06 PAGE : 16/28
---	--	---

1.2 Auxiliary data

For the TOSOMI algorithm the following auxiliary data is needed: surface albedo climatology (Combined TOMS-GOME albedo climatology) and topology database (GTOPO30). The data is specified below.

1.2.1 Specification of the GTOPO30 climatology

Originating System:	U.S. Geological Survey's EROS Data Center
Data Class	Climatology
Name of Data Source	GTOPO30
Sensor Type/Name:	N/A
Sensor key technical parameters	
Spatial resolution / coverage: 30-arc seconds	
Vertical resolution / coverage: N/A	
Temporal resolution / coverage: N/A	
System operations availability	
Start date: N/A	
End date: N/A	
Probability of availability	
100 %	
Product name and reference to product technical specification document:	
GTOPO30. Documentation at http://edcdaac.usgs.gov/gtopo30/README.asp	
Data availability and coverage:	
Time-scale: N/A	
Geographic: Global	
Further parameters and remarks:	
-	
References: http://edcdaac.usgs.gov/gtopo30/gtopo30.asp	

	Algorithm Document TOSOMI	REF : TEM/AD3/002 ISSUE : 1.0 DATE : 09.08.06 PAGE : 17/28
---	--	---

1.2.2 Specification of combined GOME/TOMS albedo climatology

Originating System:	TOMS and GOME data
Data Class	climatology
Name of Data Source	Albedo climatology from TOMS and GOME observations
Sensor Type/Name:	TOMS and GOME
Sensor key technical parameters	
Spatial resolution / coverage: 1 x 1 degree / Global	
Vertical resolution / coverage: N/A	
Temporal resolution / coverage: N/A	
System operations availability	
Start date: N/A	
End date: N/A	
Probability of availability	
100 %	
Product name and reference to product technical specification document:	
TOMS albedo data set : see GSE-PRO-IN-EO-5 and <i>Herman, J. R. and E. A. Celarier, Earth surface reflectivity climatology at 340-380 nm from TOMS data, J. Geophys. Res., 102, 28,003-28,011, 1997.</i>	
GOME albedo data set : <i>Koelemeijer, R. B. A., P. Stammes, J. W. Hovenier, and J. F. de Haan, Global distributions of effective cloud fraction and cloud top pressure derived from oxygen A band spectra measured by the Global Ozone Monitoring Experiment: comparison to ISCCP data, J. Geophys. Res., 107(D12), 4151, doi: 10.1029/2001JD000840, 2002.</i>	
Data availability and coverage:	
Time-scale: N/A	
Geographic: Global	

1.3 Sensitivity and Error analysis

See next section and and [Eskes et al., 2005]

	Algorithm Document TOSOMI	REF : TEM/AD3/002 ISSUE : 1.0 DATE : 09.08.06 PAGE : 18/28
---	--	---

1.4 Validation with groundbased observations

1.4.1 Approach

TOSOMI data from 2003 and 2004 were compared at seventy ground locations with ground-based Dobson (47), Brewer (22), or Filter (1) data. From the TOSOMI data, the nearest match for each individual ground measurements was selected, with a collocation criterium of 100 km and 12 hours. For the ground data, daily averaged ozone columns were taken, with the exception of the De Bilt and Paramaribo sites, where the measurement closest in time to the SCIAMACHY overpass was taken.

Overpass data were taken from the daily averaged ozone summary file at the WOUDC database, except Paramaribo and De Bilt data, which were taken from daily files stored in the NILU-Envisat validation database. Excluded from our comparison were stations that yielded fewer than twenty collocations with SCIAMACHY data, and two stations that from other satellite validation results were known to have large biases. No distinction between direct sun and zenith sky measurements was made.

1.4.2 Validation results

For each station, time-series of collocated SCIAMACHY and ground ozone columns, along with the percent differences, were made and plotted. From visual inspection we conclude that the overall ozone observations from the ground were well tracked by SCIAMACHY. Examples for the Arosa NH mid-latitude station, and the Syowa Antarctic station, are shown in Fig. 4 and 5. For Arosa we find a bias of -0.7% and a rms of 4.2%. For Syowa we find a bias of -0.6% and a rms of 5.3%. Arosa is a typical NH mid-latitude station, showing a large ozone variability in winter. Syowa shows a large dynamical range of ozone values due to the South Pole ozone hole, which is well captured by the TOSOMI observations.

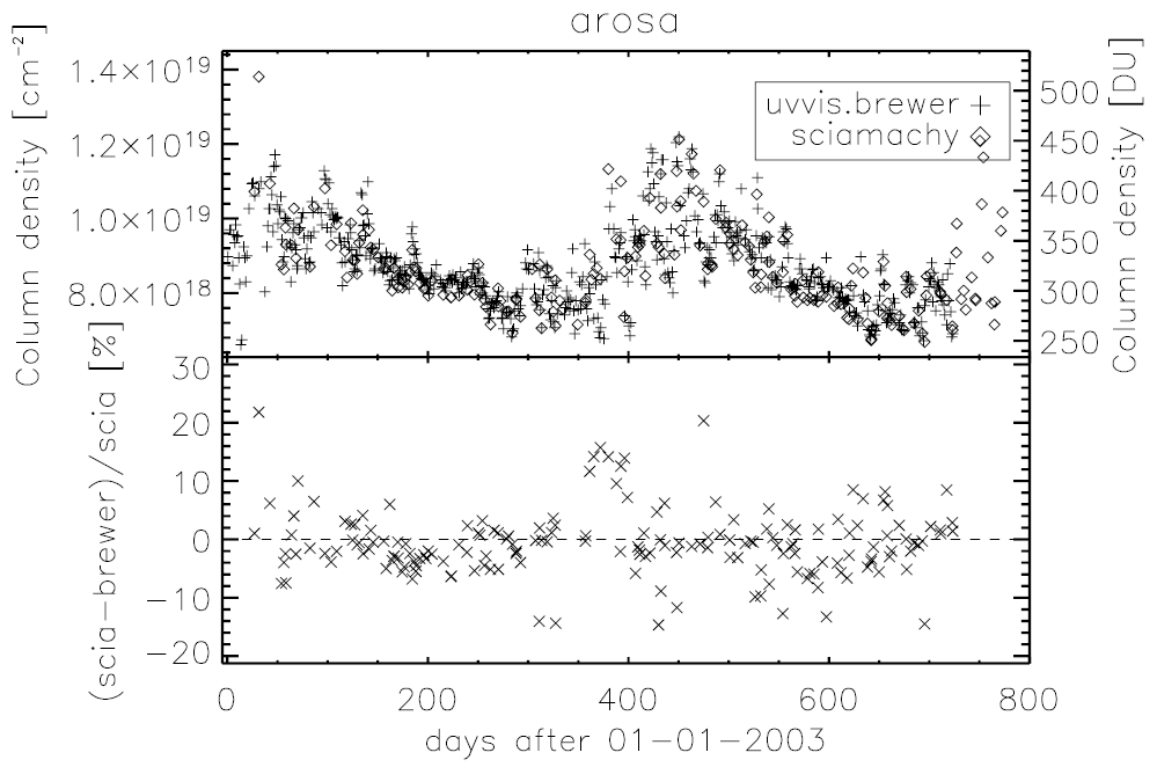


Fig. 4. Time series of Brewer ozone measurements at Arosa (46.78N, 9.68E), and collocated SCIAMACHY columns (top panel), and the relative difference between the two data sets. Relative differences are plotted for the closest matches of the satellite observations within a radius of 100 km and within 12h time difference.

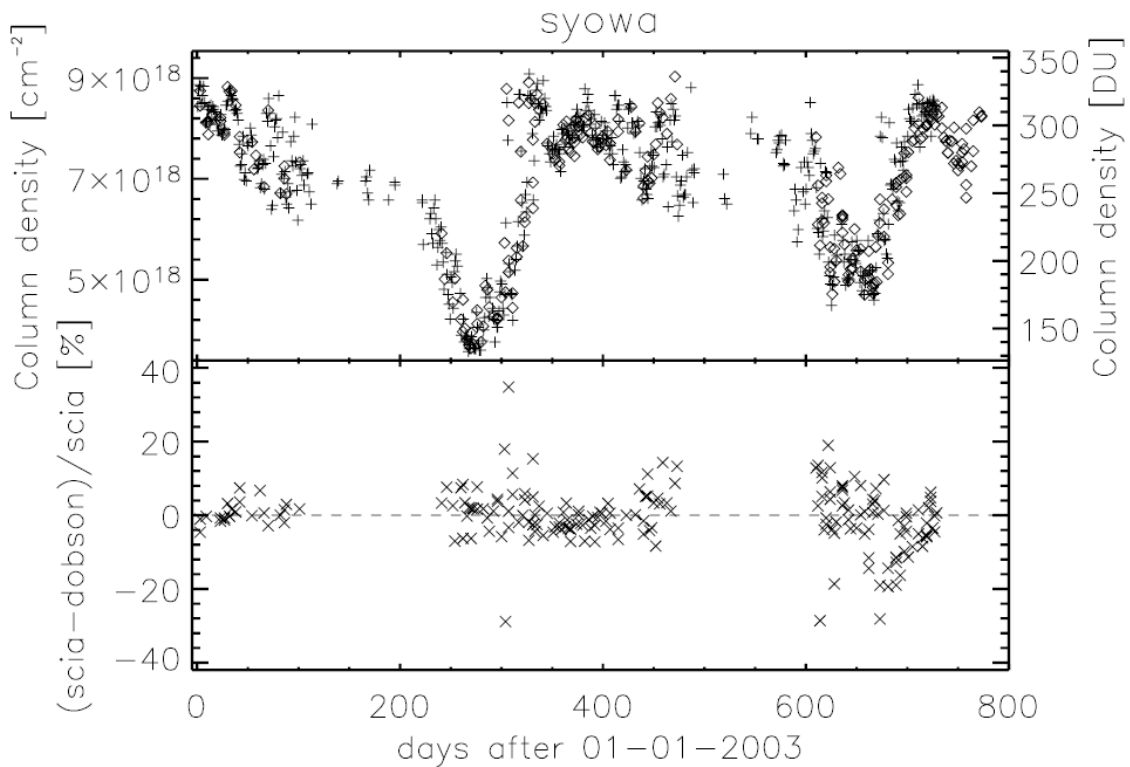


Fig. 5. Same as Figure 4, but now for the Dobson instrument of Syowa station (69.00S, 39.58E).

Time series for all comparisons are plotted on a colour scale (where colour depicts percent difference between SCIAMACHY and ground based) as a function of month (horizontally), and binned into 10 degree latitude bins (vertically). Only months with four or more comparisons are plotted, as shown in Figure 6. The most statistically significant conclusion can be drawn from the results between 30 and 60 degrees north, where 42 ground instruments, more than half of all stations listed in Table 1, have been compared. There is a small seasonal difference in the comparison results, which range from about -3 to +2%. This may be due to a seasonal dependence of the Dobson and Brewer retrievals (Van Roozendael et al., 1998). There is no evidence for a latitudinal dependence in the TOSOMI-ground based comparison. The dark blue patch in June/July of 2003 in the Arctic, is not statistically significant, since only one ground station is present in the 70-75 latitude bin (namely, Barrow at 71N), and the anomaly results from two measurement days during a time of fast ozone change.

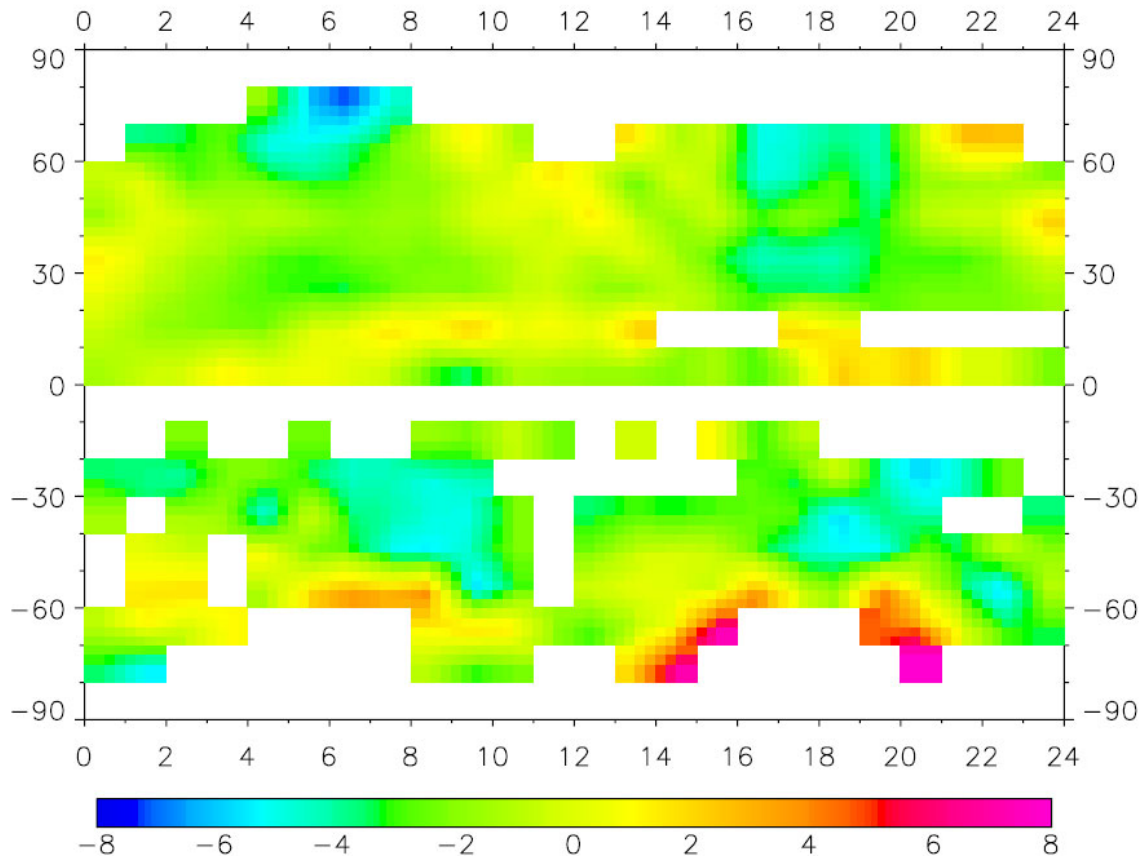


Fig. 6. Difference between TOSOMI columns and Brewer and Dobson stations in 2003 and 2004, as a function of the month since January 2003 (horizontal axis) and latitude (vertical axis). Colours show $(\text{TOSOMI} - \text{groundbased}) / \text{TOSOMI}$ in percent. Data from 68 station is binned on 10 degree latitude and 1 month boxes. Data is only shown when more than 4 collocations occur within a box.

Around the onset and end of the ozone hole over the Antarctic, TOSOMI data are clearly higher than groundbased measurements. It is unclear whether this is due to systematic effects in SCIAMACHY or the TOSOMI algorithm, or in the ground based Dobson measurements, or both. However, a recent study suggests that Dobson measurements underestimate ozone columns by 4% in ozone hole conditions for large solar zenith angles (Bernhard et al., 2005). Similar differences have also been seen when other satellite data were compared with Dobson/Brewers (Lambert and Balis, 2004). The number of ground stations in these latitude bins is one (50-60 S, Ushuaia), two (60-70 S, Marambio and Syowa), and one (70-80 S, Arrival Heights). Light blue patches (about -5%) appear between months 7 and 10, and 18 and 21, in the Southern Hemisphere at latitudes between 30 and 40 S (two stations) and 40 and 50 S (two stations). The comparison series were averaged over time, for each of the stations. Results are plotted in Fig. 7. This Figure shows that the bias between SCIAMACHY and ground based is, on average, -1.7%. There is no clear latitudinal dependence. The standard deviation on the biases is, on average, 4.4%. Here, it appears

that the rms is smallest in the tropics, and increases towards the poles. This may be due to larger and quicker ozone variations towards the poles. Average numbers presented are the mean of all individual station's results. The same data as in the top panel of this Figure are also shown on a world map, where biases are now shown in colours as presented in Fig. 8. These data are tabulated in Table 1.2.

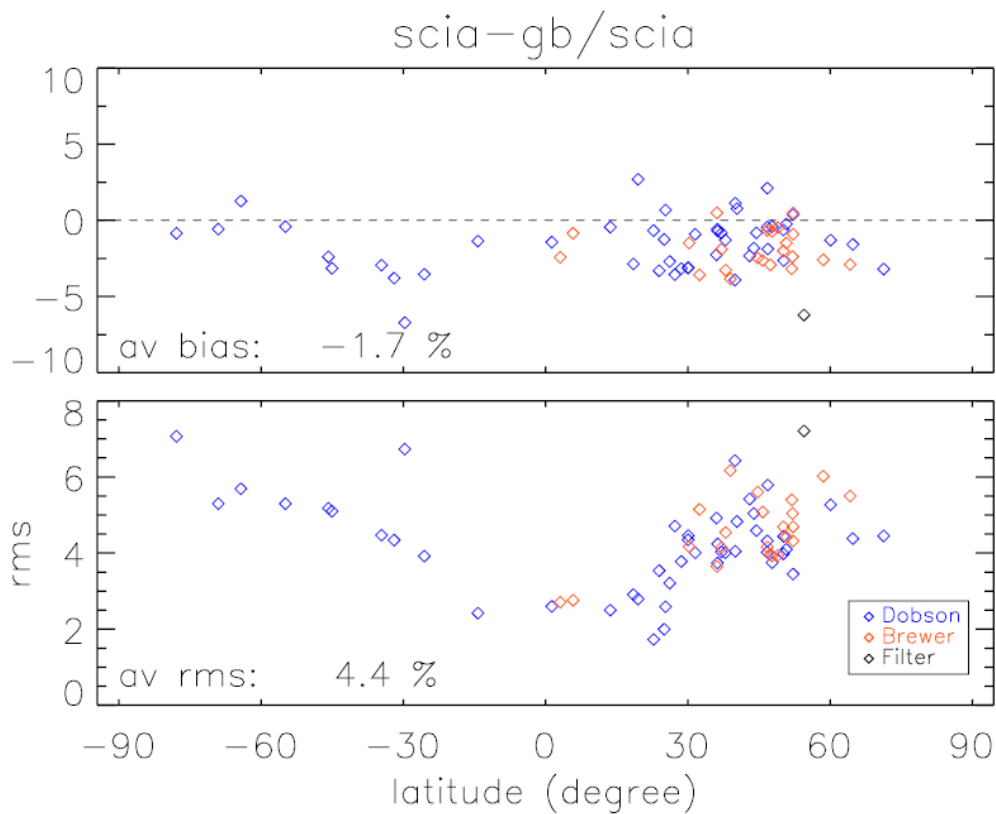


Fig. 7. World wide overview of the comparison between ground based measurements (Brewer and Dobson) and the TOSOMI retrievals, presented as a function of the latitude. Top panel: bias; bottom panel: rms, both in %.

Biases ozone column data

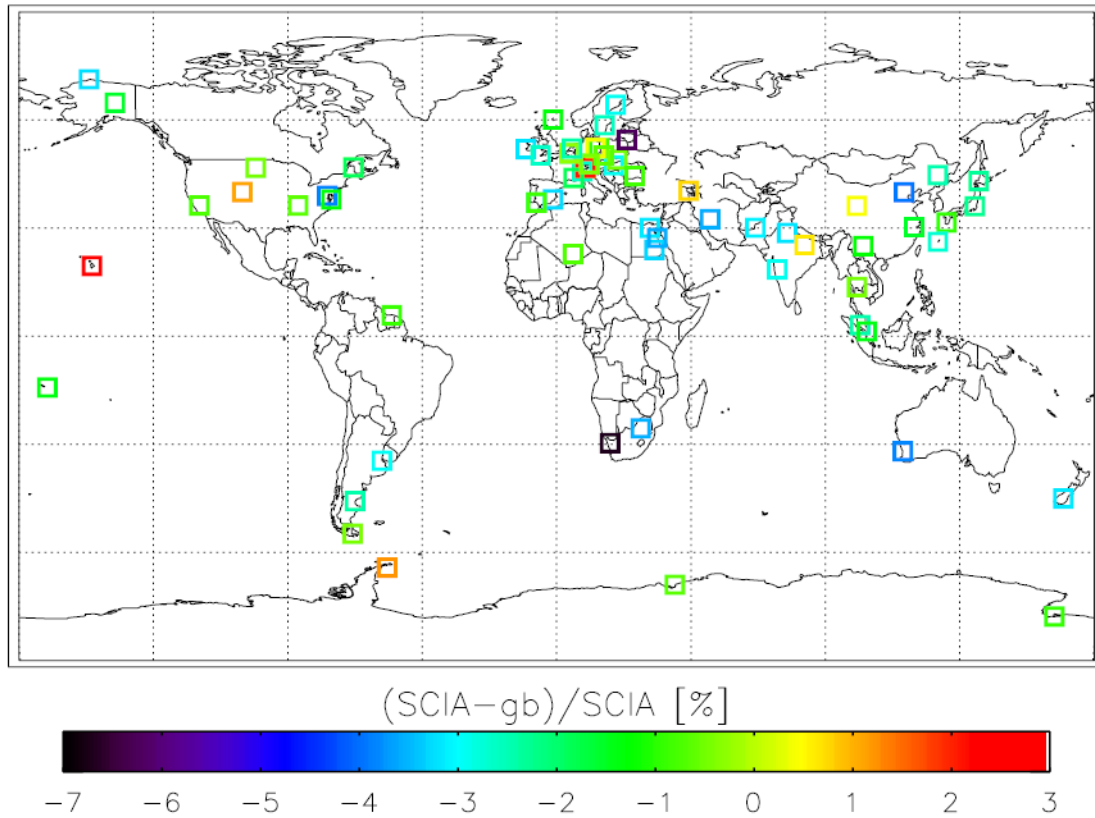


Fig. 8. A world map showing the locations of stations included in the comparison. The colours indicate the mean difference between SCIAMACHY and ground based ozone columns.

There is a good agreement between the validation results presented here and the validation reported for the TOGOMI GOME algorithm (Van Oss et al., 2004).

	Algorithm Document TOSOMI	REF : TEM/AD3/002 ISSUE : 1.0 DATE : 09.08.06 PAGE : 24/28
---	--	---

Table 1.2 List of stations included in the comparison with SCIAMACHY, their location, instrument type, bias and standard deviation with respect to TOSOMI, the correlation coefficient and the number of intercomparisons.

Location	lat	lon	instrument	bias	rms	corcoef	num
Arrival Heights	-77.83	166.67	Dobson	-0.85	7.07	0.85	81
Syowa	-69.00	39.58	Dobson	-0.57	5.30	0.94	205
Marambio	-64.23	-56.72	Dobson	1.27	5.69	0.93	84
Ushuaia	-54.85	-68.31	Dobson	-0.41	5.30	0.88	184
Comodoro Rivadavia	-45.78	-67.50	Dobson	-2.40	5.18	0.81	171
Lauder	-45.03	169.68	Dobson	-3.15	5.10	0.88	71
Buenos Aires	-34.58	-58.48	Dobson	-2.94	4.47	0.82	112
Perth	-31.92	115.95	Dobson	-3.79	4.34	0.94	101
Springbok	-29.67	17.90	Dobson	-6.72	6.73	0.88	164
Irene	-25.56	28.19	Dobson	-3.54	3.92	0.88	119
Samoa	-14.25	-170.56	Dobson	-1.36	2.42	0.57	67
Singapore	1.33	103.88	Dobson	-1.43	2.60	0.84	95
Petaling Jaya	3.10	101.65	Brewer	-2.42	2.71	0.88	123
Paramaribo	5.81	-55.21	Brewer	-0.85	2.76	0.81	142
Bangkok	13.67	100.61	Dobson	-0.44	2.50	0.92	64
Poona	18.53	73.85	Dobson	-2.86	2.91	0.95	26
Mauna Loa	19.53	-155.57	Dobson	2.70	2.79	0.94	55
Tamanrasset	22.80	5.52	Dobson	-0.67	1.73	0.90	141
Aswan	23.97	32.78	Dobson	-3.31	3.54	0.91	145
Kunming	25.03	102.68	Dobson	-1.25	2.00	0.96	64
Varanasi	25.32	83.03	Dobson	0.68	2.59	0.79	113
Naha	26.20	127.68	Dobson	-2.70	3.21	0.93	144
Hurghada	27.28	33.75	Dobson	-3.56	4.71	0.70	151
New Delhi	28.65	77.22	Dobson	-3.17	3.78	0.77	128
Cairo	30.08	31.28	Dobson	-3.14	4.35	0.79	184
Quetta	30.11	66.57	Dobson	-3.09	4.46	0.46	106
Linan	30.30	119.73	Brewer	-1.49	4.17	0.79	83
Kagoshima	31.58	130.57	Dobson	-0.91	4.01	0.85	149
Isfahan	32.48	51.42	Brewer	-3.58	5.15	0.67	166
Tateno Tsukuba	36.06	140.10	Dobson	-2.26	4.92	0.86	157
Mt Waliguan	36.17	100.53	Brewer	0.49	3.65	0.79	115
Nashville	36.25	-86.57	Dobson	-0.59	3.74	0.83	81
Hanford	36.32	-119.63	Dobson	-0.70	4.24	0.84	88
El Arenosillo	37.10	-6.73	Brewer	-1.90	4.14	0.84	160
El Arenosillo	37.10	-6.73	Dobson	-0.83	4.03	0.84	59
Wallops Island	37.93	-75.48	Dobson	-1.29	4.01	0.86	34
Murcia	38.00	-1.17	Brewer	-3.27	4.54	0.87	115
Goddard	38.99	-76.83	Brewer	-3.84	6.17	0.75	120
Xianghe	39.97	116.37	Dobson	-3.92	6.43	0.78	116
Boulder	40.03	-105.25	Dobson	1.13	4.05	0.85	81
Amberd	40.38	44.25	Dobson	0.77	4.83	0.73	71
Sapporo	43.06	141.33	Dobson	-2.33	5.42	0.87	167
Haute Provence	43.93	5.70	Dobson	-1.83	5.04	0.86	72
Bucharest	44.48	26.13	Dobson	-0.82	4.59	0.87	131
Longfengshan	44.75	127.60	Brewer	-2.47	5.60	0.87	105
JRC Ispra Varese	45.80	8.63	Brewer	-2.63	5.08	0.86	178
Bismarck	46.77	-100.75	Dobson	-0.44	4.02	0.88	121
Arosa	46.78	9.68	Brewer	-0.66	4.16	0.88	177
Arosa	46.78	9.68	Dobson	2.12	4.32	0.87	156
Caribou	46.87	-68.03	Dobson	-1.88	5.79	0.66	49
Budapest Lorinc	47.43	19.18	Brewer	-2.92	3.97	0.94	154

	Algorithm Document TOSOMI	REF : TEM/AD3/002 ISSUE : 1.0 DATE : 09.08.06 PAGE : 25/28
---	--	---

location	lat	lon	instrument	bias	rms	corcoef	num
Hohenpeissenberg	47.80	11.02	Brewer	-0.72	3.92	0.89	182
Hohenpeissenberg	47.80	11.02	Dobson	-0.40	3.75	0.91	122
Poprad-Ganovce	49.03	20.32	Brewer	-0.48	3.94	0.91	227
Hradec Kralove	50.18	15.83	Brewer	-2.01	4.69	0.87	223
Hradec Kralove	50.18	15.83	Dobson	-0.63	3.98	0.89	164
Camborne	50.22	-5.32	Dobson	-2.64	4.44	0.93	66
Uccle	50.80	4.35	Brewer	-1.49	4.42	0.88	185
Uccle	50.80	4.35	Dobson	-0.24	4.10	0.91	128
Valentia	51.93	-10.25	Brewer	-3.18	5.40	0.58	10
De Bilt	52.10	5.18	Brewer	-2.38	5.04	0.89	206
Lindenberg	52.21	14.12	Brewer	-0.91	4.69	0.84	200
Potsdam	52.22	13.05	Brewer	0.48	4.32	0.79	21
Potsdam	52.22	13.05	Dobson	0.38	3.45	0.91	19
Kaunas	54.52	23.54	Filter	-6.22	7.21	0.89	224
Norrkoeping	58.58	16.15	Brewer	-2.59	6.02	0.87	261
Lerwick	60.13	-1.18	Dobson	-1.30	5.27	0.90	154
Vindeln	64.24	19.77	Brewer	-2.90	5.50	0.90	240
Fairbanks	64.82	-147.87	Dobson	-1.58	4.38	0.92	65
Barrow	71.32	-156.60	Dobson	-3.20	4.45	0.97	42

1.5 Recommendations for product validation

see section 1.4

1.6 References

Bass and Paur. The ultraviolet cross-sections of ozone. I. The measurements. II - Results and temperature dependence, In *Proc. Quadrennial Ozone Symp.*, Chalkidiki, Greece, Eds. C. Zefros and A. Ghazi. Reidel, Dordrecht, 606p., 1986.

Bernhard, G., Evans, R. D., Labow, G. J., and Oltmans, S. J.: Bias in Dobson total ozone measurements at high latitudes due to approximations in calculations of ozone absorption coefficients and airmass, *J. Geophys. Res.* 110, D10305, doi:10.1029/2004JD005559, 2005.

Burrows, J.P., M. Weber, M. Buchwitz, V. Rozanov, A. Ladstätter-Weissenmayer, A. Richter, R. De Beek, R. Hoogen, K. Bramstedt, K.W. Eichmann, M. Eisinger, and D. Perner, The Global Monitoring Experiment (GOME): Mission concept and first scientific results, *J. Atmos Sci.*, Vol 56, 151-175, 1999a.

	Algorithm Document TOSOMI	REF : TEM/AD3/002 ISSUE : 1.0 DATE : 09.08.06 PAGE : 26/28
---	--	---

Burrows, J.P., Richter, A., Dehn, A., Deters, B., Himmelmann, S., Voigt, S., Orphal, J., Atmospheric remote-sensing reference data from GOME - 2. Temperature-dependent absorption cross sections of O₃ in the 231-794 nm range. *Journal of Quantitative Spectroscopy & Radiative Transfer*, 61, pp. 509-517. 1999b.

De Haan, J.F., P.B. Bosma, and J.W. Hovenier, The adding method for multiple scattering calculations of polarized light, *Astron. Astrophys. Vol 183*, 371-391, 1987.

De Haan, J.F., Accounting for Raman Scattering in DOAS, *SN-OMIE-KNMI-409*, KNMI, 2003.

De Rooij, W.A., van der Stap, C.C.A.H., 1984, Expansion of Mie Scattering Matrices in Generalized Spherical Functions, *Astron. & Astrophys*, Vol 131, 237-248.

Eskes, H. J., R. J. van der A, E. J. Brinksma, J. P. Veefkind, J. F. de Haan, and P. J. M. Valks, Retrieval and validation of ozone columns derived from measurements of SCIAMACHY on Envisat, *Atmos. Chem. Phys. Discuss.*, 5, 4429-4475, 2005.

Fortuin J.P.F., and H. Kelder, An ozone climatology based on ozonesonde and satellite measurements, *J. Geophys. Res.*, Vol 103, NO. D23, 31,709-31,734, 1998.

Fong, K.W., T.H. Jefferson, T. Suyehiro and L. Walton, Guide to the SLATEC Common Mathematical Library, available at: <http://www.netlib.org/slatec/guide>, 1993.

Fournier, N., Stammes, P., Acarreta, J. R., Eskes, H., Piters, A., Hess, M., von Bargaen, A., Kokhanovsky, A., and Grzegorski, M.: SCIAMACHY cloud product validation, Proceedings of the second workshop on the Atmospheric Chemistry Validation of Envisat (ACVE-2), 3-7 May 2004.

Koelemeijer, R.B.A., and P. Stammes, Effects of clouds on ozone column retrieval from GOME UV measurements, *J. Geophys. Res.*, 104, NO. D7, 8,281- 8,294, 1999.

Koelemeijer, R.B.A., Effect of Lambert surface approximation for clouds on the air mass factor of ozone in the UV, KNMI memo, March 7, 2001.

Koelemeijer, R.B.A., P. Stammes, J.W. Hovenier, and J.F. de Haan, A fast method for retrieval of cloud parameters using oxygen A-band measurements from GOME, *J. of Geophys. Res.*, 106, 3475-3490, 2001.

Koelemeijer, R.B.A., P. Stammes, J.W. Hovenier, and J.F. de Haan, Global distributions of effective cloud fraction and cloud top pressure derived from oxygen A-band spectra measured by the Global Ozone Monitoring Experiment: comparison to ISCCP data, *J. of Geophys. Res.*, 107, 4151, 2002.

Koelemeijer, R.B.A., J.F. de Haan, and P. Stammes, A database of spectral surface reflectivity in the range 335-772 nm derived from 5.5 years of GOME observations, *J. of Geophys. Res.*, 108, 4070, 2003.

Lambert, J.-C., et al., *Investigation of Pole-to-Pole Performances of Spaceborne Atmospheric Chemistry Sensors with the NDSC*, *J. Atm. Sci.*, 56, 1999.

	Algorithm Document TOSOMI	REF : TEM/AD3/002 ISSUE : 1.0 DATE : 09.08.06 PAGE : 27/28
---	--	---

Lambert, J.-C. and D. Balis: Delta validation report for ERS-2 GOME Data Processor upgrade to version 4.0, ERSE-CLVL-EOPG-TN-04-0001, Version 1.0, <http://wdc.dlr.de/sensors/gome/gdp4/validation.pdf>, ESA, December 2004.

Levelt, P.F., and co-authors, Science Requirements Document for OMI-EOS, RS-OMIE-KNMI-001, Version 2, ISBN 90-369-2187-2, 2000.

Martin, R.V., K. Chance, D.J. Jacob, T.P. Kurosu, R.J.D. Spurr, E. Bucsela, J.F. Gleason, P.I. Palmer, I. Bey, A.M. Fiore, Q. Li, R.M. Yantosca, and R.B.A. Koelemeijer, An improved retrieval of tropospheric nitrogen dioxide from GOME, *J. Geophys. Res.*, 107, 4437, 2002.

Mishchenko, M.I., and L. D. Travis, Capabilities and limitations of a current FORTRAN implementation of the T-matrix method for randomly oriented, rotationally symmetric scatterers, *J. Quant. Spectrosc. Radiat. Transfer*, Vol 60, 309-324, 1998

More, J. J., The Levenberg-Marquardt algorithm: implementation and theory. In Numerical Analysis Proceedings (Dundee, June 28 - July 1, 1977, G. A. Watson, Editor), *Lecture Notes in Mathematics 630*, Springer-Verlag, 1978.

Orphal, J., A critical review of the absorption cross-sections of O₃ and NO₂ in the 240-790 nm region, ESA Technical Note MO-TN-ESA-GO-0302, 2002.

Schutgens N.A.J., and P. Stammes, Parametrisation of Earth's polarisation spectrum from 290 to 330 nm, *J. Quantitative Spectroscopy and Radiative Transfer*, 239-255, 2002.

Spurr, R., W. Thomas and D. Loyola, GOME Level 1 to 2 Algorithms Description, DLR Technical note ER-TN-DLR-GO-0025, Rev. 3/A, Oberpfaffenhofen, Germany, 2002.

Stammes, P., J.F. de Haan, and J.W. Hovenier, The polarized internal radiation field of a planetary atmosphere, *Astron. Astrophys. Vol 225*, 239-259, 1989

Stammes, P., Spectral radiance modelling in the UV-Visible range, to appear in: *IRS 2000: Current problems in Atmospheric Radiation*, Eds. W.L. Smith and Y.M. Timofeyev, A. Deepak Publ., Hampton (VA), 2001.

Valks, P., J. P. Veefkind, J. F. de Haan, and R. van Oss, *TOGOMI Algorithm Theoretical Baseline Document*, TOGOMI/KNMI/ATBD/001, Issue 1.2, 01/11/2003.

Valks, P., and R. van Oss, TOGOMI Algorithm Theoretical Basis Document, Issue 1.2, TOGOMI/KNMI/ATBD/001, KNMI/ESA, November 2003, http://www.gse-promote.org/services/ozone_nrt/togomi_ATBD_v1.21.pdf.

Van der A, R., Recalibration of GOME spectra for the purpose of ozone profile retrieval, *Technical Report TR-236*, KNMI, De Bilt, The Netherlands, 2001.

Van de Hulst, H.C., Multiple Light Scattering. Tables, Formulas and Applications. Academic Press, San Diego, Ca., pp 573-577, 1980.

	Algorithm Document TOSOMI	REF : TEM/AD3/002 ISSUE : 1.0 DATE : 09.08.06 PAGE : 28/28
---	--	---

Van Geffen, J.H.G.M., Documentation of the software package GomeCal (version 1.0), *Technical report TR-255, KNMI, De Bilt, The Netherlands, 2003a.*

Van Geffen, J.H.G.M. and R.F. Van Oss, Wavelength calibration of spectra measured by GOME using a high-resolution reference spectrum, *Applied Optics*, 42, 2739-2753, 2003b.

van Oss, R. F., Valks, P. J. M., and de Haan, J. F.: TOGOMI Delta Validation Document, TOGOMI/KNMI/VAL/002, KNMI/ESA, January 2004, http://www.gse-promote.org/services/ozone_nrt/togomi_deltavalidation_v1.0.pdf.

Van Roozendael, M., Peeters, P., Roscoe, H.K., de Backer, H., Jones, A. E., Bartlett, L., Vaughan, G., Goutail, F., Pommereau, J.-P., Kyro, E., Wahlstrom, C., Braathen, G., and Simon, P. C.: Validation of ground-based visible measurements of total ozone by comparison with Dobson and Brewer spectrophotometers, *J. Atmosp. Chem.*, 29, 55-83, 1998.

Van Roozendael, V. Soebijanta, C.Fayt, and J.-C. Lambert, Investigation of DOAS issues affecting the accuracy of the GDP version 3.0 total ozone product, in *ERS-2 GOME GDP 3.0 Implementation and Delta Validation Report*. Issue 1.0, 2002.

Veeffkind, J.P., Temperature effects on ozone slant column density, draft 2, *Tech. Rep.*, TN-OMIE-KNMI-234, KNMI, De Bilt, The Netherlands, 2000a.

Veeffkind, J.P., Effects of instrument signal-to-noise on ozone DOAS, *Tech. Rep.*, TN-OMIE-KNMI-239, KNMI, De Bilt, The Netherlands, 2000b.

Veeffkind, J.P., Effect of ozone profile shape on the slant column density, *Tech. Rep.*, TN-OMIE-KNMI-232, KNMI, De Bilt, The Netherlands, 2000c.

Veeffkind, J.P. and J.F. de Haan, OMI Algorithm Theoretical Basis Document, Barthia, P.K (ed), Volume II - Chapter 3, DOAS Total Ozone Algorithm, *ATBD-OMI-02*, Version 1.0, September 2001.

Veeffkind, J.P. and J.F. de Haan, OMI Algorithm Theoretical Basis Document, Barthia, P.K (ed), Volume II - Chapter 3, DOAS Total Ozone Algorithm, *ATBD-OMI-02*, Version 2.0, http://www.knmi.nl/omi/documents/data/OMI_ATBD_Volume_2_V2.pdf, August 2002.